Review Article

Nonlinear frequency response analysis: a recent review and perspectives

Tanja Vidaković-Koch[1], Tamara Miličić[1], Luka A. Živković[1],
Hoon Seng Chan[2], Ulrike Krewer[2] and Menka Petkovska[3]

Abstract

The nonlinear frequency response analysis (NFRA) can be seen as an extension of electrochemical impedance spectroscopy. NFRA gives a full and detailed representation of the system response and can establish a connection between model parameters and the experimentally observed phenomena. In this article, different theoretical NFRA approaches and the most recent application examples are discussed. A simple electrochemical example is used to showcase the benefits and disadvantages of analyzing the system response by using different approaches. In addition, it was shown how to extract experimental harmonic values and analyze them.

Addresses

[1] Max Planck Institute for Dynamics of Complex Technical Systems, Electrochemical Energy Conversion, Magdeburg, Germany
[2] Karlsruhe Institute of Technology, Institute for Applied Materials – Electrochemical Technologies, Karlsruhe, Germany
[3] University of Belgrade, Faculty of Technology and Metallurgy, Belgrade, Serbia

Corresponding author: Vidakovi ć -Koch, Tanja (vidakovic@mpi-magdeburg.mpg.de)

Keywords
Harmonic analysis, Diagnosis, Kinetics, MModel discrimination, Battery.

Electrochemical systems are inherently nonlinear. Therefore, linear frequency response analysis leads to the loss of important information on system dynamics, a problem that is well-recognized in the case of electrochemical impedance spectroscopy (EIS). As demonstrated in different publications, an extension of dynamic analysis to the nonlinear range provides full information for proper system diagnostics [1–4]. In addition, nonlinear analysis is highly beneficial for the analysis of reaction mechanisms, model discrimination, and parameter determination [2].

The nonlinear dynamic analysis is termed differently within the electrochemical community. It is known as faradaic rectification (FR) [5,6], nonlinear EIS (NLEIS), total harmonic distortion (THD) [3,7], or nonlinear frequency response analysis (NFRA, NFR analysis) [1,2,8]. In all these methods, a single input change was used. If multiple inputs (e.g. at different input frequencies) are implemented, the nonlinear dynamic analysis is termed intermodulated differential immittance spectroscopy [9]. The term NLEIS is most often used focusing on either nonlinearity at fundamental frequency [10] or nonlinearities in the second and higher-order harmonics [4,11]. The popularity of this term can be explained by the relationship/similarity of an experimental procedure to EIS, therefore this method is considered as an extension of EIS to the nonlinear range. But as discussed by some authors [12], the response function 'impedance' has meaning only for the fundamental frequency and higher-order response functions cannot be defined in the same way as impedance. Therefore, for contributions at higher frequencies, a more general term is better suited. THD adds up all higher harmonics and relates them to the fundamental harmonic, thus merging and losing detailed information [7]. NFRA aims to describe the full nonlinear response including the nonperiodic part of the response (FR in older publications), nonlinear contributions at the fundamental frequency, as well as nonlinear contributions at higher harmonic frequencies [13,14]. In addition, NFRA can treat multiple inputs and describe intermodulated contributions (the focus of intermodulated differential immittance spectroscopy), see for example [15]. While NLEIS and NFRA constrain the extent of the input amplitude to control the number of higher-order harmonics in the response, THD does not impose such restrictions.

Since the 1950s, different groups have studied various aspects of nonlinearities in electrochemical measurements [5,16]. However, there is still no consensus in the theoretical and experimental analysis of data obtained by high input amplitude studies. Therefore, in this article, theoretical backgrounds, followed by experimental determination of nonlinear part of the response

and recent application examples are discussed. The focus is on a single input/single output case.

Theoretical backgrounds

To analyze experimental NFR data, apart from phenomenological correlations [17,18], numerical [19] and analytical approaches [13,14,20] have been suggested in the literature. Both approaches build on mechanistic models. To support a comparative discussion of these approaches, a simple model of an electrochemical interface is introduced:
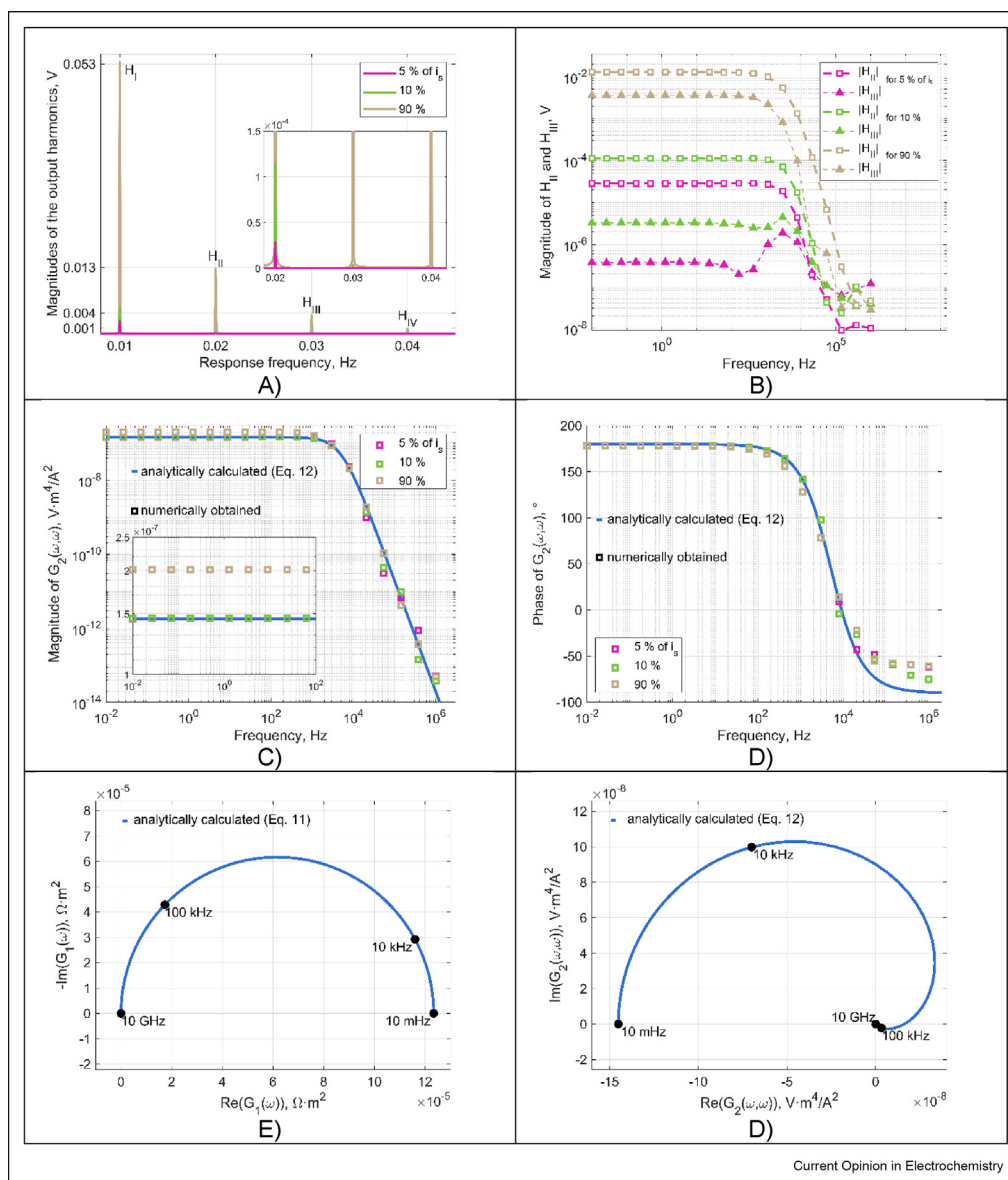
$$c_{DL}\frac{dE(t)}{dt} = i(t) - i_F(t) \qquad (1)$$

where c_{DL} is the double layer capacity, $E(t)$ is potential, $i(t)$ is the cell current density, and $i_F(t)$ is the faradaic current defined according to Butler−Volmer equation:

$$i_F(t) = i_o \bullet \left[e^{\alpha_A \bullet f \bullet E(t)} - e^{\alpha_C \bullet f \bullet E(t)} \right] \qquad (2)$$

With α_A, α_C being anode and cathode transfer coefficients, i_o exchange current, $f = F/(RT)$ with F

Figure 1

Comparison of numerical and analytical approaches of NFR and overview of different types of data presentation. Fourier transform of numerically obtained potential output (**a**), numerical second and third harmonics for different amplitude values, expressed in % of steady state current i_s (**b**), amplitude (**c**) and phase (**d**) of analytical (Eq. (12)) and numerical second order FRFs and analytical first (**e**) and second order (**f**) FRF in Nyquist plot. All data are calculated for i_s = 374 A m^{-2} (corresponds to E_s = 0.1 V), c_{DL} = 0.2 F m^{-2}, i_o = 55.5 A m^{-2}, $\alpha_A = \alpha_C$ = 0.5, R = 8.314 J mol^{-1} K^{-1}, T = 293.15 K, F = 96,485 C mol^{-1}. NFR, nonlinear frequency response; FRF, frequency response function.

being the Faraday constant, R the universal gas constant, and T temperature.

In general, the NFR of a weakly nonlinear system to a periodic input deflection,

$$u(t) = u_s + A \cdot cos(\omega \cdot t) = u_s + \frac{A}{2} \cdot \left(e^{j \cdot \omega \cdot t} + e^{-j \cdot \omega \cdot t}\right) \quad (3)$$

Can be represented in form of a Fourier series:

$$
\begin{aligned}
y_{qs}(t) - y_s = y_{DC} + &\underbrace{H_I(\omega, A) \cdot e^{j \cdot \omega \cdot t} + H_I(-\omega, A) \cdot e^{-j \cdot \omega \cdot t}}_{h_I(t)} \\
+ &\underbrace{H_{II}(2\omega, A) \cdot e^{j \cdot 2\omega \cdot t} + H_{II}(-2\omega, A) \cdot e^{-j \cdot 2\omega \cdot t}}_{h_{II}(t)} \\
+ &\underbrace{H_{III}(3\omega, A) \cdot e^{j \cdot 3\omega \cdot t} + H_{III}(-3\omega, A) \cdot e^{-j \cdot 3\omega \cdot t}}_{h_{III}(t)} + \dots
\end{aligned}
$$

$$(4)$$

where $u(t)$ is either potential or current, A is the amplitude of input change around its steady-state value u_s, $y_{qs}(t)$ is the periodic quasi-steady state of the output (current or potential), y_s the steady-state value of the output, y_{DC} the DC contribution of the NFR (FR in older publications), and h_i, H_i $(i = I, II, \dots, \infty)$ the harmonics of the NFR in the time and frequency domain, respectively. In the numerical NFR approach [8,19], the nonlinear system response (Eq. (4)) is mapped into the frequency domain via a discrete Fourier transformation (Figure 1a). In Figure 1b, second and third harmonics as a function of frequency and input signal amplitude are shown. Wolff et al. [19] showed that the second and third harmonics contain important information on the reaction kinetics/mass transfer and react differently to a change in a steady-state, (u_s), and an asymmetry of the kinetics, that is, α_A, $\alpha_C \neq 0.5$ (see discussion in the following). This high sensitivity to kinetics and surface may be used for battery state diagnosis [8].

While the numerical approach determines only amplitude-dependent harmonics [19], the analytical approach gives input-amplitude—independent analytical expressions of higher-order frequency response functions (FRFs) [13]. The analytical approach based on the Volterra series and the Fourier transform is explained here in more detail [1,2,21,22]. A somewhat similar approach was suggested by McDonald and Adler [23] and used also by others [20].

One can show that the terms in Eq. (4) can be expressed as [24]:

$$y_{DC} = 2 \cdot \left(\frac{A}{2}\right)^2 \cdot G_2(\omega, -\omega) + 6 \cdot \left(\frac{A}{2}\right)^4 \cdot G_4(\omega, \omega, -\omega, -\omega)$$
$$+ \dots$$

$$(5)$$

$$H_I(\omega, A) = \left(\frac{A}{2}\right) \cdot G_1(\omega) + 3 \cdot \left(\frac{A}{2}\right)^3 \cdot G_3(\omega, \omega, -\omega) + \dots$$

$$(6)$$

$$H_{II}(2\omega, A) = \left(\frac{A}{2}\right)^2 \cdot G_2(\omega, \omega) + 4 \cdot \left(\frac{A}{2}\right)^4 \cdot G_4(\omega, \omega, \omega, -\omega)$$
$$+ \dots$$

$$(7)$$

With the leading terms, $G_2(\omega, -\omega)$ being asymmetrical 2nd-order FRF, $G_1(\omega)$ the 1st-order FRF, and $G_2(\omega, \omega)$ the symmetrical 2nd-order FRF. The procedure for the theoretical derivation of FRFs is straightforward and well-documented in the literature [1,2,21,22]. The FRFs derived for the simple electrochemical interface (Eqs. (1) and (2)) and different output/input combinations are summarized in Table 1. For simplicity, only expressions for $G_1(\omega)$, $G_2(\omega, \omega)$, and $G_2(\omega, -\omega)$ are shown. Other FRFs can be obtained by following the same methodology.

In Table 1, R_1 equals:

Table 1

Overview of different inputs/outputs and theoretical frequency response functions.

Output/Input	Theoretical frequency response function	Unit	Eq.
$i(t)$ / $E(t)$	$G_1(\omega) = c_{DL}j\omega + \dfrac{1}{R_1}$	A m^2 V^{-1}	8
	$G_2(\omega, \omega) = \dfrac{f}{R_2}$	A m^2 V^{-2}	9
	$G_2(\omega, -\omega) = \dfrac{f}{R_2}$	A m^2 V^{-2}	10

(*continued on next page*)

Table 1 (*continued*)

Output/Input	Theoretical frequency response function	Unit	Eq.
$E(t)/i(t)$	$G_1(\omega) = \dfrac{R_1}{R_1 \cdot c_{DL} \cdot j \cdot \omega + 1}$	V A^{-1} m^2	11
	$G_2(\omega, \omega) = \dfrac{-\dfrac{f}{R_2}}{\left(2 \cdot c_{DL} \cdot j \cdot \omega + \dfrac{1}{R_1}\right) \cdot \left(c_{DL} \cdot j \cdot \omega + \dfrac{1}{R_1}\right)^2}$	V A^{-2} m^4	12
	$G_2(\omega, -\omega) = \dfrac{\dfrac{f}{R_2}}{\dfrac{1}{R_1} \cdot \left[(c_{DL} \cdot j \cdot \omega)^2 - \left(\dfrac{1}{R_1}\right)^2\right]}$	V A^{-2} m^4	13
$i(t)/E_{input}(t)$	$G_1(\omega) = \dfrac{c_{DL} \cdot j \cdot \omega + \dfrac{1}{R_1}}{1 + R_\Omega\left(c_{DL} \cdot j \cdot \omega + \dfrac{1}{R_1}\right)}$	A m^2 V^{-1}	14
	$G_2(\omega, \omega) = \dfrac{\dfrac{f}{R_2}}{\left[1 + R_\Omega\left(c_{DL} \cdot j \cdot \omega + \dfrac{1}{R_1}\right)\right]^2 \left[1 + R_\Omega\left(2 c_{DL} \cdot j \cdot \omega + \dfrac{1}{R_1}\right)\right]}$	A m^2 V^{-2}	15
	$G_2(\omega, -\omega) = \dfrac{\dfrac{f}{R_2}}{\left[\left(1 + \dfrac{R_\Omega}{R_1}\right)^2 - (c_{DL} \cdot j \cdot R_\Omega \cdot \omega)^2\right]\left[1 - \dfrac{R_\Omega}{R_1}\right]}$	A m^2 V^{-2}	16

$$R_1 = \frac{1}{i_o \cdot [\alpha_A \cdot e^{\alpha_A \cdot f \cdot E_s} + \alpha_C \cdot e^{-\alpha_C \cdot f \cdot E_s}] \cdot f} \qquad (17)$$

And R_2:

$$R_2 = \frac{2}{i_o \cdot [\alpha_A^2 \cdot e^{\alpha_A \cdot f \cdot E_s} - \alpha_C^2 \cdot e^{-\alpha_C \cdot f \cdot E_s}] \cdot f} \qquad (18)$$

R_1, R_2 are related to coefficients of the Taylor series approximation of Eq. (2). R_1 is defined as a linear charge transfer resistance, while R_2 is the nonlinear resistance (for potential input) (Eqs. (9) and (10)). $G_1(\omega)$ for the same output/input combination correspond to the reciprocal value of each other, admittance (Eq. (8)) versus impedance (Eq. (11)). This is no longer true for the second-order FRFs. In general, $G_2(\omega, \omega)$ and $G_2(\omega, -\omega)$ contain different information, but in some cases, they can be identical (Eqs. (9) and (10), Table 1). In a symmetrical system $\alpha_A = \alpha_C$ and for equilibrium conditions ($E_s = 0$), $G_2(\omega, \omega)$ and $G_2(\omega, -\omega)$ will be zero. Similar was shown numerically [15], and also analytically [23]. This simple case visualizes that non-linearities are caused by nonlinear kinetics [10,25], but they also depend on steady-state conditions. One of the conclusions of many previous studies is that the second-order FRF is free of double-layer capacitance and Ohmic resistance contributions because these effects are largely linear [25]. Although this reasoning appears straightforward, it is not correct. In general, double-layer capacitance and the Ohmic resistance influence second and higher-order FRFs. This is because the input potential always contains Ohmic drop contribution (please note that for the derivation of Eqs. (8)−(10), it was assumed that $R_\Omega = 0$) in accordance to:

$$\Delta E_{input}(t) = \Delta E(t) + R_\Omega \Delta i(t) \qquad (19)$$

where R_Ω is the Ohmic resistance. It follows that potential ($\Delta E(t)$) is no longer an ideal cosine input (Eq. (3)), but an auxiliary output containing contributions of higher-order harmonics. An addition of Eq. (19) makes an original model (Eqs. (1) and (2)) complex, therefore one can show that Eq. (8) will modify to

$$G_1(\omega) = \left\{c_{DL}j\omega + \frac{1}{R_1}\right\} G_{1,E}(\omega) \qquad (20)$$

where

$$G_{1,E}(\omega) = 1 - R_\Omega G_1(\omega) \qquad (21)$$

Is an auxiliary output, obtained from Eq. (19) after substitution of inputs and outputs and application of the harmonic probing (please see steps 5 and 6 in the *Supplementary Information*). As one can see an addition of further model equations (Eq. (22)) complicates the original model, therefore, the $G_1(\omega)$ function will now be calculated from Eqs. (20) and (21) (please see

Table 1 for the final expression). Similarly, the expressions for other FRFs can be obtained (Table 1). One can easily see that both $G_2(\omega, \omega)$ and $G_2(\omega, -\omega)$ will be influenced by double-layer capacitance and Ohmic layer resistance (Table 1 Eqs.(15) and (16)). All theoretical FRFs (Table 1) are derived assuming no mass transfer limitations. In presence of mass transfer limitations, the original dynamic model of the system should be extended by mass balance equations, as shown in our previous publications [1,13]. As a consequence, new auxiliary outputs (for concentration changes) will be defined, increasing the size of the system of equations to be solved. The detailed procedure and the analytical expressions for FRFs, including mass transfer effects, as well as Ohmic resistances, can be seen in our previous publications [1,13]. As has been shown, mass transfer limitations will cause additional nonlinearities in the system response [1,13].

As the higher-order FRFs contain kinetic parameters in different combinations than the first-order FRF, NFRA allows identifying more kinetic parameters than EIS. In addition, the shapes of $G_2(\omega, \omega)$ [13] and $G_2(\omega, -\omega)$ [14] are often unique for a certain mathematical model. Therefore, higher-order FRFs and higher-order harmonic responses will be more sensitive to model discrimination [2,13]. $G_2(\omega, -\omega)$ is a dominant part of y_{DC} (Eq. (5)). Positive $G_2(\omega, -\omega)$ values result in higher reaction rate values, that is, current, under periodic operation than steady-state operation [14].

The amplitude and phase of $G_2(\omega, \omega)$ for current as the input (Eq. (12), Table 1) are visualized in Figure 1c and d. To compare analytical expressions with numerically calculated data (Figure 1b), it was assumed that $G_2(\omega, \omega)$ is the dominant part of the second harmonic (see Eq. (7)). Then one can write:

$$G_2(\omega, \omega) = \frac{2 \cdot H_{II}(2\omega, A)}{A^2} \qquad (22)$$

This assumption is satisfied at low input amplitude values (5 and 10% of the steady-state value, Figure 1c. At higher input amplitudes (90%), the contributions of higher harmonics become significant. In general, when using numerical data, sufficient discretization of the time signal is required to avoid disturbance of the frequency response by noise especially at high frequencies; this also applies to experiments. Besides Bode plots, Nyquist diagrams are also common (Figure 1e) [20].

The derivation of FRFs for models of higher complexity is straightforward, but it requires both time and specific mathematical skills from the user, thus making its application unappealing to beginners. Here, a purely numerical approach may be used (see

above). Alternatively, software for automatic derivation of analytical FRFs; the so-called computer-enhanced NFR (cNFR) was introduced by Zivkovic et al. [26]. The feasibility of the cNFR method was already demonstrated for experimental identification of the oxygen reduction reaction (ORR) [8]. This software enables fast and automatic derivation of all analytical FRFs of interest through a user-friendly modeling interface. Most importantly, cNFR generated FRF files allow for smooth integration with existing numerical algorithms, the result of which is fast parameter estimation for the competing reaction mechanisms, and optimization of the operating variables [27].

Experimental determination

Providing that one can obtain experimental current or potential output signal in the time domain [4,13], the harmonics in the output, as well as the aperiodic term, can be gained by Fast Fourier transform. Alternatively, some frequency response analyzers offer harmonics directly [24]. In the latter case, there is no information on the aperiodic part of the response. In the numerical NFR approach, harmonics from the output are directly compared with harmonics from experiments [28]. Experimental FRFs can be also determined from aperiodic contribution and first- and higher-order harmonics and compared with theoretical descriptions (Table 1). The procedure for $G_2(\omega, \omega)$ is already explained in an example of numerical data (Eq. (22)). Similarly, assuming that leading terms in Eqs. (5) and (6) are dominant ones, $G_2(\omega, -\omega)$ and $G_1(\omega)$ can be obtained from experimental data according to the study by Panic et al. [24], Lin and Ng [29]:

$$G_2(\omega, -\omega) = \frac{2 \cdot y_{DC}}{A^2} \qquad (23)$$

$$G_1(\omega) = \frac{H_I(\omega, A)}{A} \qquad (24)$$

where y_{DC} the aperiodic contribution appears at zero frequency in the Fast Fourier transform spectra together with the steady-state part of the response.

Recent NFR applications

The recent focus of NFR analysis is on kinetic studies and batteries. Kandaswamy et al. [13] and Zivkovic et al. [14] studied ORR on silver in alkaline solutions. It was shown that the simple kinetics (first electron transfer as a rate-determining step and mass transport limitations) describes ORR in 0.1 M NaOH solution well. Good qualitative agreement between theoretical and experimental FRFs was observed for the first-order FRF $G_1(\omega)$ (Figure 2a and b) and second-order FRF $G_2(\omega, \omega)$ (Figure 2b and c) [13], as well as for DC components (Figure 2d) [14]. In a very concentrated alkaline

Figure 2
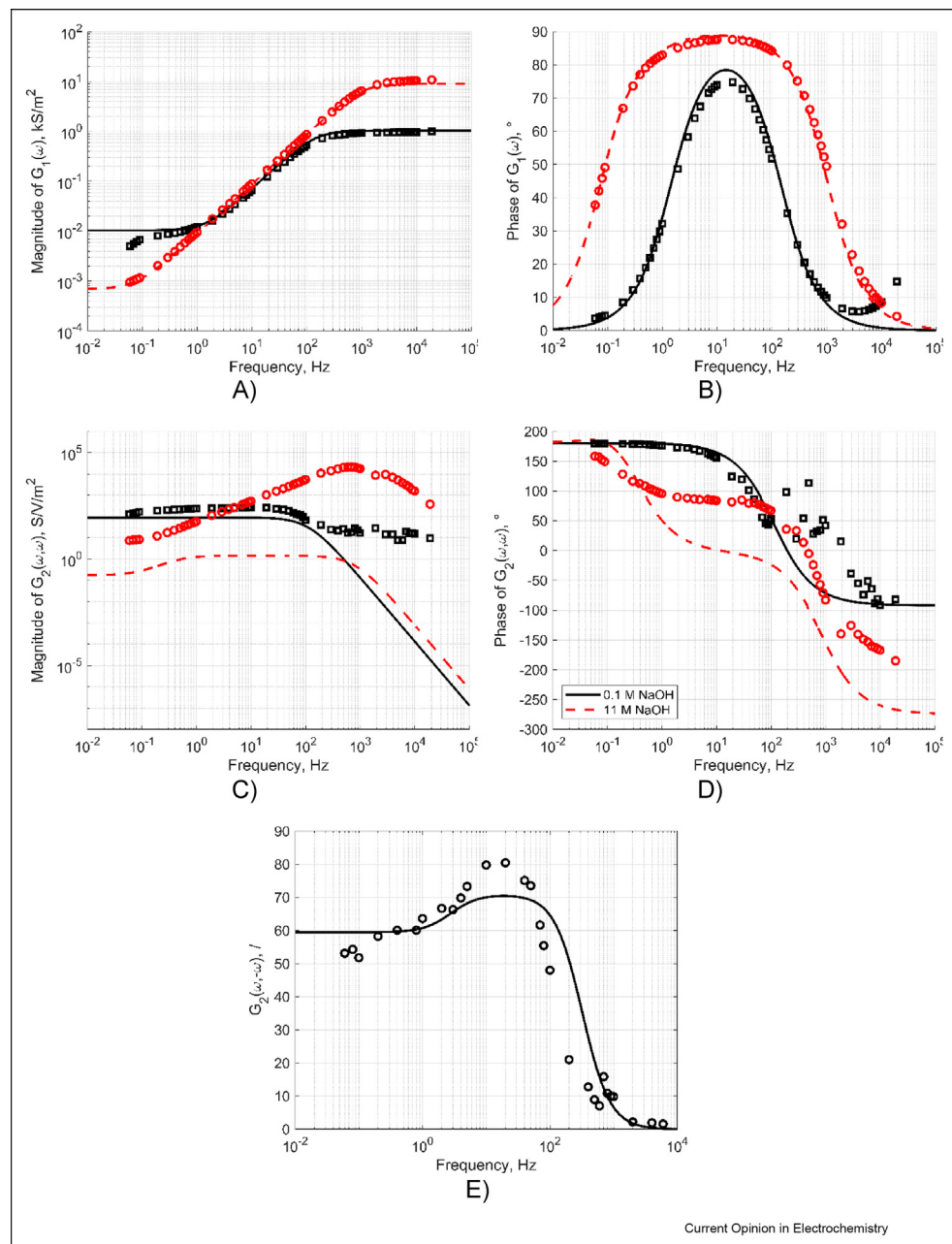
Comparison of the analytically derived (solid line), and experimentally obtained FRFs (symbols), (**a**) magnitude of the 1st-order FRF; (**b**) phase of the 1st-order FRF; (**c**) magnitude of the symmetrical 2nd-order FRF; (**d**) phase of the symmetrical 2nd-order FRF; (**e**) the asymmetrical 2nd-order FRF. Input is potential, and output is current density at two different NaOH concentrations: 0.1 M and 11 M NaOH (black and red, respectively). Redrawn based on data in the study by Kandaswamy et al. [13] and Zivkovic et al. [14]. FRF, frequency response function.

solution (11 M NaOH), the simple kinetics describes well, the linear region (Figure 2a and b), but in the second-order FRF, the agreement is not so good (Figure 2c and d). Therefore a more advanced model representation is required for the description of ORR kinetics in concentrated alkaline solution. Zivkovic et al. [14] studied theoretically the potential of different inputs (potential, rotation rate) concerning process intensification. The positive value of $G_2(\omega, -\omega)$ for a specific output/input combination indicates process improvement, while the negative value deterioration. It was shown that for potential input process improvement can be obtained (Figure 2e), while for rotation rate as an input, the process cannot be improved (not shown here). With help of theoretical FRF, it was explained that diffusion layer thickness under forced periodic

Figure 3
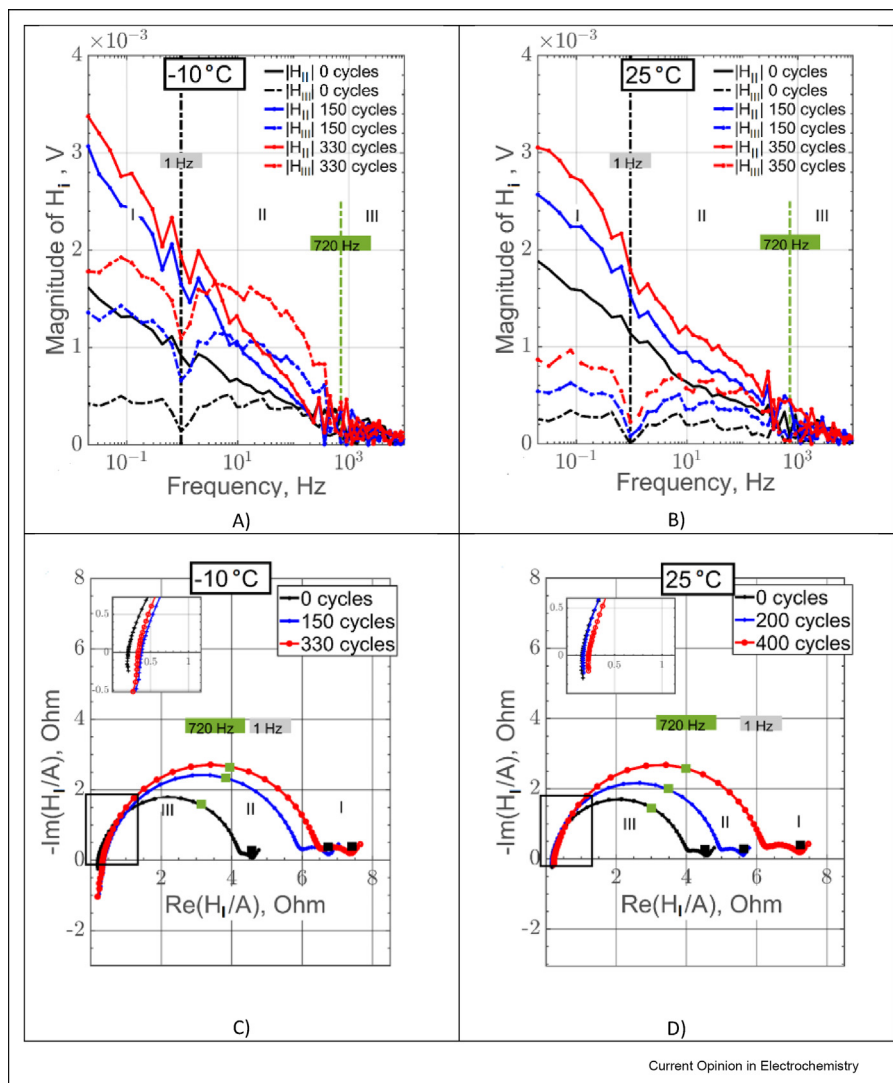
Experimental NFR data (second and third harmonics) of Li-ion battery aged under lithium plating. (**a**) and without lithium plating (**b**), as well as input signal amplitude normalized first harmonic in Nyquist plot presentation under lithium plating (**c**) and without lithium plating (**d**). Redrawn from the study by Harting et al. [18]. NFR, nonlinear frequency response.

operation will be always thicker than under steady-state conditions (lower oxygen concentration at the interface), which will lead to negative $G_2(\omega, -\omega)$, that is, process deterioration.

Dynamic methods are widely used for the analysis and diagnosis of (Li-ion) batteries [30]. Similarly, as in fuel cells [3,31,32], nonlinear methods improve the feasibility to discriminate among different battery processes and degradation issues. Whereas both, experimental EIS and NFR spectra could be divided into three characteristic frequency regions, NFRA revealed negligible nonlinearities at high frequencies, that is, the dynamics stem not only from electrochemical reactions but also Li-ion transfer through the solid-

electrolyte interphase [33]. Temperature, amplitude, and aging [33] impacted the spectra, as well as state of charge [20], DC bias [34], and compression pressure [35]. State-of-health could be predicted by analyzing various NFRA features [17,36]; machine learning even allowed to minimize error below 4% [17]. Furthermore, NFRA outperformed EIS as it enabled us to distinguish between normal aging and aging because of the safety-critical Li-plating [18]; only for plated cells, the third harmonics was higher than the second one (Figure 3). Quantitative experimental interpretation poses challenges, as NFR spectra of different batteries may vary strongly, both qualitatively and quantitatively [28,37]. Model-based parameter sensitivity studies allowed to elucidate the impact of material parameters, for

example, diffusion or reaction constants, and thus transport or reaction processes on NFR spectra [19,28,38]. Special care should further be taken to guarantee a quasi-steady-state, as transient behavior may impact spectra especially at low frequencies [8].

Conclusions and perspectives

NFRA allows in-depth kinetic studies and diagnosis of electrochemical surfaces. In-depth interpretation of spectra requires physical models, limiting its widespread application presently. NFR approach used in the study by Kandaswamy et al. [13] and Zivkovic et al. [14] offers a unified treatment of all parts of the nonlinear response, and it is easily adaptable to models of electrochemical systems of different complexity and different output/input combinations (also nonelectrical). Software-assisted tools, such as cNFR [26], can accelerate the broader application of analytical approaches.

Numerical NFR analysis is easy to implement [33], but care has to be taken to achieve a periodic (quasi) steady-state in simulations. FRFs can be obtained from numerical harmonic values. It was shown that if amplitude in numerical simulations is a well-selected agreement between analytically derived and numerically obtained FRFs can be achieved. Numerical simulations give also useful guidance for the design of the experiment (e.g. selection of amplitude).

FRFs have often unique shapes (both experimental and theoretical) and contain a unique combination of process parameters, two features that make higher-order FRFs valuable for model discrimination.

Although experimentally NFR is similar to EIS, the experimental routines need to be better established for broader use.

Currently, the NFR is focused on kinetics and batteries, and in the past, it was also used for fuel cell studies [3,31,32]. However, the method can be easily applied to other electrochemical systems (e.g. electrolyzers). Currently, mainly the second and third harmonic, as well as the symmetrical second-order FRF were in focus. The asymmetrical, second-order FRF, the main contribution of a nonperiodic DC component was largely overlooked part of the NFR. Its significance in different applications, for example, in model discrimination or as a measure of process improvement under forced periodic operation, compared with the steady-state operation, still has to be demonstrated.

Declaration of competing interest

The authors declare that they have no known competing financial interests or personal relationships that could

have appeared to influence the work reported in this paper.

Appendix A. Supplementary data

Supplementary data to this article can be found online at https://doi.org/10.1016/j.coelec.2021.100851.

References

Papers of particular interest, published within the period of review, have been highlighted as:

* of special interest
** of outstanding interest

1. ** Vidaković-Koch TR, Panić VV, Andrić M, Petkovska M, Sundmacher K: **Nonlinear frequency response analysis of the ferrocyanide oxidation kinetics. Part I. A theoretical analysis**. *J Phys Chem C* 2011, **115**:17341−17351.
    Analytical NFR approach application on an example of simple electrochemical reaction.

2. ** Bensmann B, Petkovska M, Vidaković-Koch T, Hanke-Rauschenbach R, Sundmacher K: **Nonlinear frequency response of electrochemical methanol oxidation kinetics: a theoretical analysis**. *J Electrochem Soc* 2010, **157**:B1279.
    Analytical NFR approach application on an example of complex electrochemical reaction.

3. Mao Q, Krewer U: **Total harmonic distortion analysis of oxygen reduction reaction in proton exchange membrane fuel cells**. *Electrochim Acta* 2013, **103**:188−198.

4. Wilson JR, Schwartz DT, Adler SB: **Nonlinear electrochemical impedance spectroscopy for solid oxide fuel cell cathode materials**. *Electrochim Acta* 2006, **51**:1389−1402.

5. Oldham KB: **Faradaic rectification: theory and application to the Hg22+/Hg electrode**. *Trans Faraday Soc* 1957, **53**:80−90.

6. Baranski AS, Diakowski PM: **High frequency faradaic rectification voltammetry at microelectrodes**. *J Phys Chem B* 2006, **110**:6776−6784.

7. Mao Q, Krewer U, Hanke-Rauschenbach R: **Total harmonic distortion analysis for direct methanol fuel cell anode**. *Electrochem Commun* 2010, **12**:1517−1519.

8. Wolff N, Harting N, Henrich M, Krewer U: **Nonlinear frequency response analysis on lithium-ion batteries: Process identification and differences between transient and steady-state behavior**. *Electrochim Acta* 2019, **298**:788−798.

9. Battistel A, La Mantia F: **Nonlinear analysis: the intermodulated differential immittance spectroscopy**. *Anal Chem* 2013, **85**:6799−6805.

10. Darowicki K: **Corrosion rate measurements by non-linear electrochemical impedance spectroscopy**. *Corrosion Sci* 1995, **37**:913−925.

11. Xu N, Riley DJ: **Nonlinear analysis of a classical system: the Faradaic process**. *Electrochim Acta* 2013, **94**:206−213.

12. Wong DKY, MacFarlane DR: **Harmonic impedance spectroscopy. Theory and experimental results for reversible and quasi-reversible redox systems**. *J Phys Chem* 1995, **99**: 2134−2142.

13. Kandaswamy S, Sorrentino A, Borate S, Živković LA, Petkovska M, Vidaković-Koch T: **Oxygen reduction reaction on silver electrodes under strong alkaline conditions**. *Electrochim Acta* 2019, **320**, 134517.

14. Živković LA, Kandaswamy S, Petkovska M, Vidaković-Koch T: **Evaluation of electrochemical process improvement using the computer-aided nonlinear frequency response method: oxygen reduction reaction in alkaline media**. *Front Chem* 2020, **8**:981.

15. Petkovska M, Marković A: **Fast estimation of quasi-steady states of cyclic nonlinear processes based on higher-order frequency response functions. Case study: cyclic operation of an adsorption column**. *Ind Eng Chem Res* 2006, **45**:266−291.

16. Fasmin F, Srinivasan R: **Review—nonlinear electrochemical
* impedance spectroscopy**. *J Electrochem Soc* 2017, **164**: H443−H455.
It offers summary of NFR studies up to 2017.

17. Harting N, Schenkendorf R, Wolff N, Krewer U: **State-of-Health identification of lithium-ion batteries based on nonlinear frequency response analysis: first steps with machine learning**. *Appl Sci* 2018, **8**:821.

18. Harting N, Wolff N, Krewer U: **Identification of lithium plating in
* * lithium-ion batteries using nonlinear frequency response analysis (NFRA)**. *Electrochim Acta* 2018, **281**:378−385.
The paper reveals the unique discriminative power of NFRA for battery state and health diagnosis.

19. Wolff N, Harting N, Röder F, Heinrich M, Krewer U: **Under-
* * standing nonlinearity in electrochemical systems**. *Eur Phys J Spec Top* 2019, **227**:2617−2640.
The paper gives a fundamental numerical analysis on how reaction and diffusion impact the second and third harmonics.

20. Murbach MD, Hu VW, Schwartz DT: **Nonlinear electrochemical
* impedance spectroscopy of lithium-ion batteries: experimental approach, analysis, and initial findings**. *J Electrochem Soc* 2018, **165**:A2758−A2765.
Model-based NFR study on batteries, revealing strong sensitivity of second harmonic to symmetry of charge transfer reactons.

21. Petkovska M, Nikolić D, Seidel-Morgenstern A: **Nonlinear frequency response method for evaluating forced periodic operations of chemical reactors**. *Isr J Chem* 2018, **58**:663−681.

22. Brzić D, Petkovska M: **A study of applicability of nonlinear frequency response method for investigation of gas adsorption based on numerical experiments**. *Ind Eng Chem Res* 2013, **52**:16341−16351.

23. McDonald TJ, Adler S: **(Invited) theory and application of
* nonlinear electrochemical impedance spectroscopy**. *ECS Transactions* 2012, **45**:429−439.
Analytical NFR approach application to solid oxide fuel cell electrode reactions.

24. Panić VV, Vidaković-Koch T, Andrić M, Petkovska M, Sundmacher K: **Nonlinear frequency response analysis of the ferrocyanide oxidation kinetics. Part II. Measurement routine and experimental validation**. *J Phys Chem C* 2011, **115**: 17352−17358.

25. Harrington DA: **Theory of electrochemical impedance of surface reactions: second-harmonic and large-amplitude response**. *Can J Chem* 1997, **75**:1508−1517.

26. Živkovic LA, Vidaković-Koch T, Petkovska M: **Computer-aided nonlinear frequency response method for investigating the dynamics of chemical engineering systems**. *Processes* 2020, **8**:1354.

27. Živković LA, Milić V, Vidaković-Koch T, Petkovska M: **Rapid multi-objective optimization of periodically operated processes based on the computer-aided nonlinear frequency response method**. *Processes* 2020, **8**, 1357.

28. Wolff N, Harting N, Heinrich M, Röder F, Krewer U: **Nonlinear frequency response analysis on lithium-ion batteries: a model-based assessment**. *Electrochim Acta* 2018, **260**: 614−622.

29. Lin RM, Ng TY: **A new method for the accurate measurement
* of higher-order frequency response functions of nonlinear structural systems**. *ISA Trans* 2018, **81**:270−285.
Although the example is from mechanical engineering, the described methodology is interesting and can be applied in electrochemical systems.

30. Krewer U, Röder F, Harinath E, Braatz RD, Bedürftig B, FIndeisen R: **Review—dynamic models of Li-ion batteries for diagnosis and operation: a review and perspective**. *J Electrochem Soc* 2018, **165**:A3656−A3673.

31. Kadyk T, Hanke-Rauschenbach R, Sundmacher K: **Nonlinear frequency response analysis of PEM fuel cells for diagnosis of dehydration, flooding and CO-poisoning**. *J Electroanal Chem* 2009, **630**:19−27.

32. Kadyk T, Hanke-Rauschenbach R, Sundmacher K: **Nonlinear frequency response analysis for the diagnosis of carbon monoxide poisoning in PEM fuel cell anodes**. *J Appl Electrochem* 2011, **41**:1021−1032.

33. Harting N, Wolff N, Röder F, Krewer U: **Nonlinear frequency response analysis (NFRA) of lithium-ion batteries**. *Electrochim Acta* 2017, **248**:133−139.

34. Ernst S, Heins TP, Schlüter N, Schröder U: **Capturing the current-overpotential nonlinearity of lithium-ion batteries by nonlinear electrochemical impedance spectroscopy (NLEIS) in charge and discharge direction**. *Front Energy Res* 2019, **7**.

35. Liebhart B, Satzke M, Komsiyska L, Snidsch C: **Application of nonlinear impedance spectroscopy for the diagnosis of lithium-ion battery cells under various operating conditions**. *J Power Sources* 2020, **480**:228673.

36. Harting N, Wolff N, Röder F, Krewer U: **State-of-Health diagnosis of lithium-ion batteries using nonlinear frequency response analysis**. *J Electrochem Soc* 2019, **166**:A277−A285.

37. Kim SH, Lee HM, Shin YJ: **Aging monitoring method for lithium-ion batteries using harmonic analysis**. *IEEE Trans Instrum Meas* 2021, **70**:1−11.

38. Murbach MD, Schwartz DT: **Extending newman's pseudo-two-dimensional lithium-ion battery impedance simulation approach to include the nonlinear harmonic response**. *J Electrochem Soc* 2017, **164**:E3311−E3320.